Nanoscale Advances

ROYAL SOCIETY OF CHEMISTRY

PAPER

View Article Online
View Journal

Cite this: DOI: 10.1039/d6na00128a

Nonlinear photophysics of PDA-based nanofluid: a potential candidate for two-photon photothermal therapy

Priyadarshi Sahoo,[a] Manika Dandapat,[a] Amit Kumar Pradhan,[b] Prasanta Kumar Datta[b] and Umakanta Tripathy*[a]

This study reports the synthesis and nonlinear photophysical characterization of polydopamine (PDA)-based nanofluid derived from dopamine (DA) monomers. The nanofluid's nonlinear photophysical behaviour was systematically examined using the Z-scan technique under both CW and fs laser excitations. Under CW excitation, the samples exhibited strong thermo-optical nonlinearities with self-defocusing, primarily due to the high photothermal conversion efficiency of PDA, which induces significant thermal lensing. In contrast, fs laser excitation induced optical nonlinearities at both 500 nm and 660 nm, where the nanofluid demonstrated positive refractive behaviour characteristic of self-focusing, accompanied by positive absorptive responses arising from two-photon absorption (TPA). The combination of efficient TPA and superior photothermal conversion suggests promising applicability in two-photon photothermal cancer therapy, enabling precise, localized heating with reduced risk to surrounding healthy tissue. Additionally, the broad nonlinear response range positions PDA-based nanofluid as a candidate for photonic applications, including all-optical switching and modulation. Optical limiting studies further confirmed its capability to protect sensitive optical systems from high-intensity laser exposure.

Received 17th February 2026
Accepted 11th May 2026

DOI: 10.1039/d6na00128a

rsc.li/nanoscale-advances

Introduction

Polydopamine (PDA)-based materials have emerged as a promising class of bioinspired polymers, garnering significant attention across diverse biomedical domains, including biosensing, bioimaging, and cancer therapeutics.[1–6] This interest stems from their exceptional physicochemical characteristics, such as strong and universal surface adhesion, remarkable aqueous dispersibility, rich chemical reactivity, intrinsic biocompatibility and biodegradability, high drug-loading capacity, and outstanding photothermal conversion efficiency.[1,2,5–7] Taken together, these attributes make PDA-based materials highly versatile, enabling their use both as carriers for advanced drug delivery systems and as functional agents for photothermal therapy (PTT), diagnostic imaging, and biosensing applications.[1,2,8–10]

Inspired by the adhesive mechanisms of mussel foot proteins, PDA is synthesized through the oxidative self-polymerization of dopamine (DA) in mildly alkaline conditions. Despite extensive research, the exact molecular mechanism underlying the oxidative self-polymerization of DA remains not fully understood. A widely accepted pathway suggests that DA is initially oxidized by dissolved oxygen to generate dopamine quinone. This intermediate then undergoes intramolecular cyclization to produce 5,6-dihydroxyindole (DHI). The subsequent formation of PDA is believed to result from a combination of covalent polymerization and non-covalent interactions between 5,6-dihydroxyindole and quinone-derived intermediates. These processes collectively drive the self-assembly of DA into the final PDA structure. Under controlled conditions, PDA can be assembled into stable nanoparticles, which enhance its applicability in targeted drug delivery and functional nanomaterial design.[1,2,11] This combination of natural inspiration and tunable synthetic versatility underpins PDA's broad potential across biomedical, environmental, and material science domains.

Among the distinct advantages of PDA is its ability to absorb broadly across the visible and near-infrared (NIR) regions, providing it with a remarkable photothermal conversion efficiency. Upon exposure to NIR irradiation, PDA nanoparticles (NPs) efficiently convert absorbed optical energy into localized heat, producing hyperthermia that is capable of targeting and eliminating cancer cells, an approach recognized as photothermal therapy (PTT).[12–17] Beyond photothermal applications, PDA has also significantly influenced drug-delivery research, primarily due to its surface chemistry. Functional groups, particularly amine and catechol residues, allow PDA surfaces to

[a]Department of Physics, Indian Institute of Technology (Indian School of Mines) Dhanbad, Dhanbad-826004, Jharkhand, India. E-mail: utripathy@iitism.ac.in
[b]Department of Physics, Indian Institute of Technology Kharagpur, Kharagpur-721302, West Bengal, India

be readily modified or functionalized, facilitating effective loading of therapeutic molecules *via* mechanisms such as π–π interactions or hydrogen bonding.[1,18–22] Furthermore, PDA-based nanocarriers exhibit controlled, stimuli-responsive drug release in response to external triggers, including pH, redox conditions, or NIR irradiation. Consequently, PDA serves as a versatile framework for developing multifunctional nanoplatforms capable of integrated therapeutic modalities such as chemo-photothermal, photodynamic-photothermal, and immuno-photothermal combinations. These synergistic treatment methods offer enhanced anti-cancer efficacy while simultaneously reducing issues related to drug resistance and cancer recurrence.[23–28] Given the diverse biomedical applications of PDA, we, to the best of our knowledge, have undertaken the first investigation of its nonlinear photophysical properties. Understanding these nonlinear photophysical behaviours holds significant potential for further advancing therapeutic methodologies based on nonlinear optics. In this study, we synthesized a PDA-based nanofluid and systematically explored its nonlinear photophysical properties using the Z-scan technique.

The Z-scan technique represents a highly versatile and widely adopted experimental method for quantifying nonlinear optical (NLO) parameters such as the nonlinear refractive index (NLR) and the nonlinear absorption coefficient (NLA).[29,30] Since its original development by Sheikh-Bahae *et al.*, the method has gained considerable prominence across multiple disciplines, including materials science, photonics, and biophysics.[31–41] Fundamentally, the Z-scan is a single-beam technique that exploits the spatial distortion of an intense laser beam as it propagates through a medium, whether solid or liquid, exhibiting nonlinear optical behaviour.[29,42] The technique is generally classified into two configurations: open-aperture (OA) and closed-aperture (CA) Z-scan. In the OA configuration, all transmitted light emerging from the sample is collected using a convex lens and subsequently directed toward the detector, enabling the evaluation of nonlinear absorption processes. In contrast, the CA configuration introduces an aperture before the detector, restricting detection to a limited portion of the transmitted beam and thereby facilitating the measurement of nonlinear refraction. In both configurations, the transmitted intensity is typically recorded in the far field to characterize the material's nonlinear optical response with high precision.[29,30,43]

Here, the nonlinear photophysical behaviour of the PDA-based nanofluid was investigated across two distinct regimes. First, thermally induced nonlinearity was examined using the CA Z-scan technique under continuous wave (CW) laser excitation. Second, to probe ultrafast nonlinear responses, femtosecond (fs) laser excitation sources at two different wavelengths (500 nm and 660 nm) were employed, with both CA and OA Z-scan configurations. This integrated approach enabled a comprehensive assessment of the PDA-based nanofluid's nonlinear photophysical properties across both thermal and ultrafast regimes, providing valuable insights into its potential for advanced photonic and biomedical applications.

Results and discussion

UV-vis absorption spectroscopy of DA and PDA

The UV-vis absorption spectra of DA and PDA are presented in Fig. 1. The spectrum of the pure DA solution in a water–ethanol mixture displays a distinct absorption peak at approximately 280 nm. Upon the addition of NaOH, DA undergoes oxidative self-polymerization, initiating the formation of PDA nanoparticles (NPs) in the solution. UV-vis spectra were recorded at different time intervals following NaOH introduction to monitor the progression of polymerization and confirm the eventual formation of PDA NPs. After 1 hour of stirring, the reaction yielded a stable dispersion of PDA NPs, as verified by the spectral data. Fig. 1 illustrates that, as PDA nanoparticles form, the UV-vis spectrum evolves into a significantly broader profile. This broadening is a direct consequence of dopamine's oxidative polymerization, which produces a structurally disordered, eumelanin-like polymer composed of catechol, quinone, and indole-like subunits. The heterogeneous arrangement of these chromophoric units generates multiple overlapping electronic transitions, resulting in the characteristic broad absorption that spans the ultraviolet, visible, and near-infrared regions.[44–48]

HRTEM imaging

Fig. 2(A) and (B) present HRTEM images of the synthesized PDA NPs, providing a clear visualization of their size. Fig. 2(C) displays the corresponding number-frequency histogram illustrating the particle size distribution derived from these images. Image analysis of 100 individual nanoparticles revealed an average particle diameter of approximately 4 nm, confirming the nanoscale dimensions and relatively narrow size distribution of the PDA NPs.

Nonlinear study using the Z-scan technique

Under CW laser excitation. This study investigates the nonlinear photophysical behaviour of DA and PDA-based

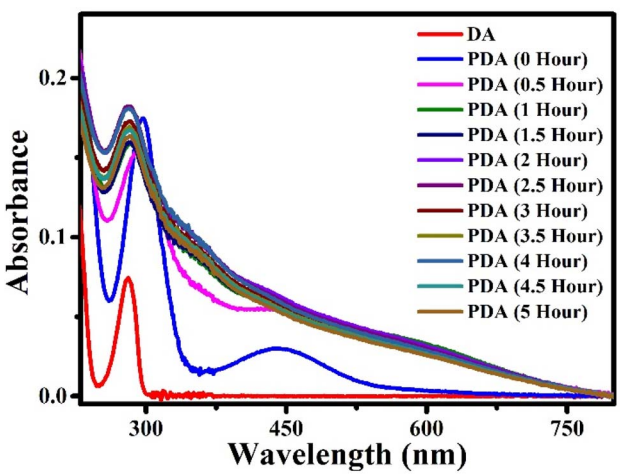

Fig. 1 The UV-vis absorption spectra of pure DA solution and dispersion of PDA NPs in the solvent (PDA-based nanofluid) at different stirring times.

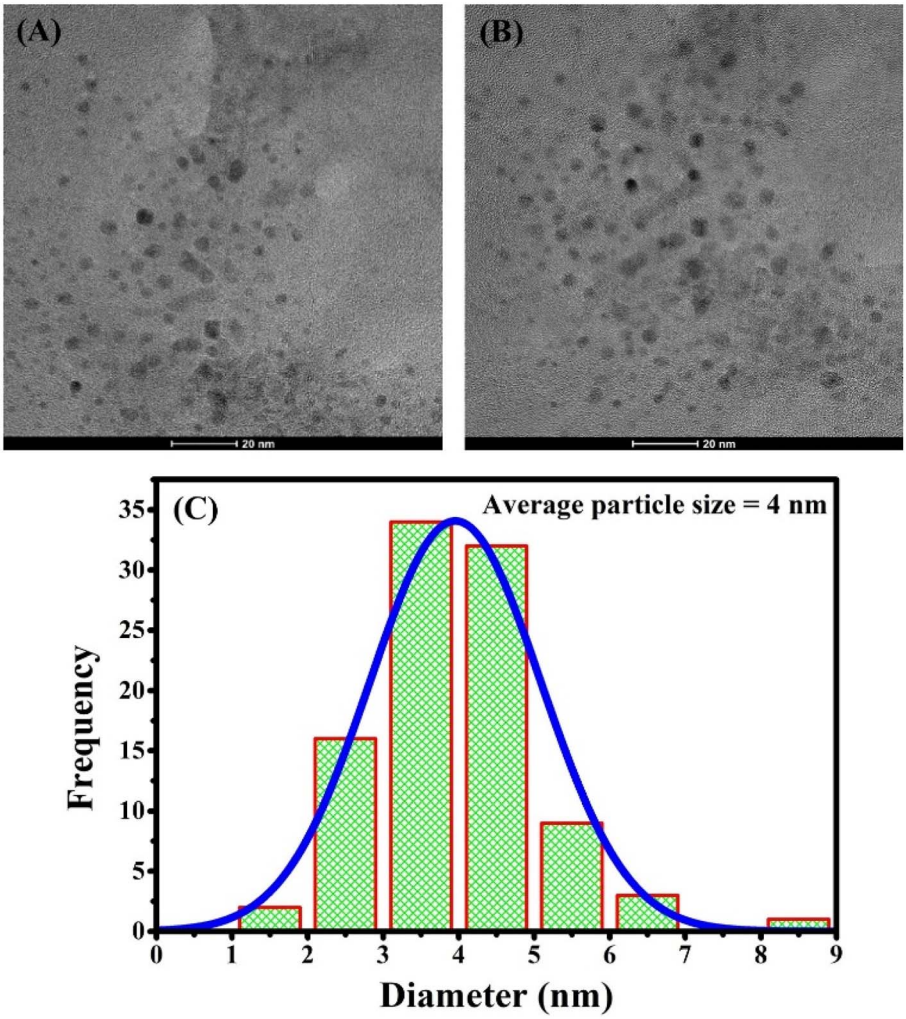

Fig. 2 Panels (A) and (B) present the HRTEM images of the PDA nanoparticles, while panel (C) illustrates the number-frequency histogram depicting the particle size distribution of the synthesized PDA NPs.

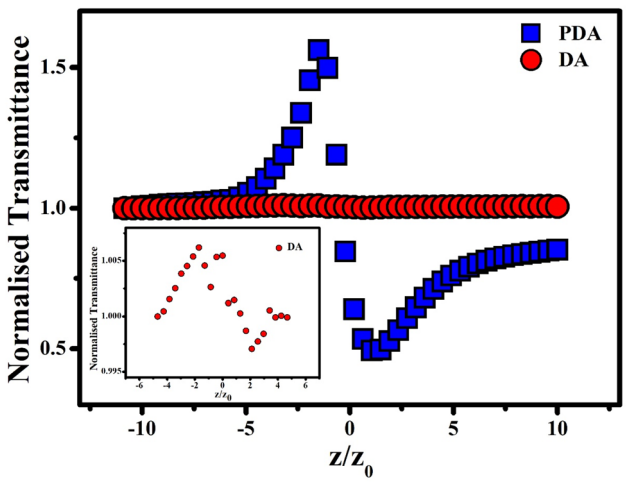

Fig. 3 CA Z-scan signals of pure DA and PDA-based nanofluid at 80 mW laser power. The inset provides a magnified view of the CA Z-scan signal for DA.

nanofluid using the CA Z-scan technique under CW laser excitation at a wavelength of 532 nm. Experiments were initially conducted on DA and the synthesized PDA-based nanofluid using a laser power of 80 mW. For a meaningful comparison, the DA solution was prepared in a water–ethanol mixture with a DA concentration (~261 μM) identical to that used for synthesizing the PDA-based nanofluid, ensuring consistency in experimental conditions. The outcomes of the CA Z-scan measurements are presented in Fig. 3, where normalized Z-scan traces for DA and PDA-based nanofluid are plotted in a single graph to facilitate direct comparison. The inset of Fig. 3 presents a magnified view of the nonlinear signal observed for pure DA. The Z-scan trace of both DA and PDA-based nanofluid displays the characteristic peak–valley signature, which is indicative of a negative nonlinear refractive index (n_2) associated with a self-defocusing effect.[29,30,49,50] The experimental data clearly show that, at the same concentration, the DA solution exhibits a much weaker nonlinear response than the PDA-based nanofluid. Specifically, the normalized peak-to-valley transmittance difference (ΔT_{P-V}) value for DA is 0.00913, while for

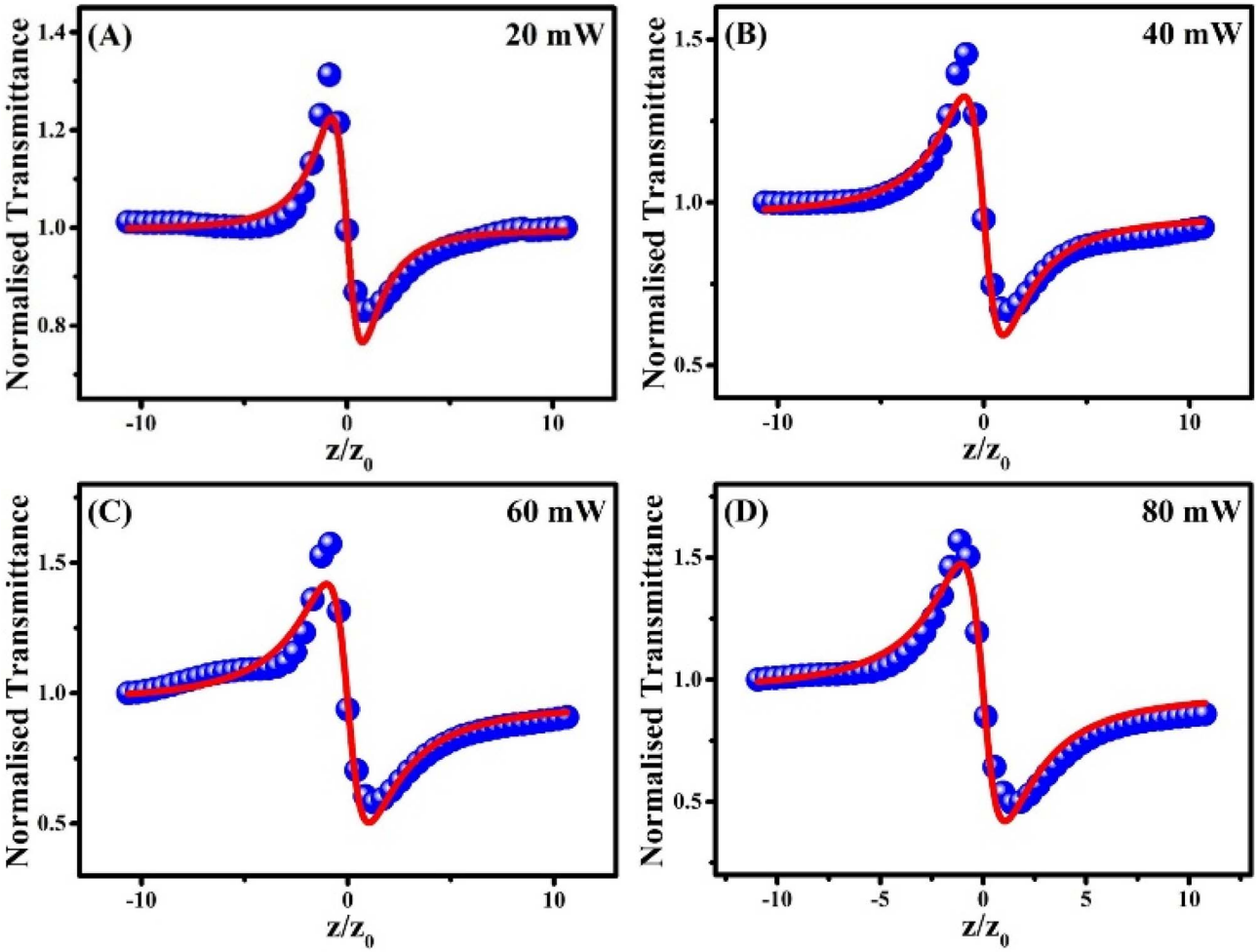

Fig. 4 CA Z-scan profiles of PDA-based nanofluid at different input laser powers: (A) 20 mW, (B) 40 mW, (C) 60 mW, and (D) 80 mW. The blue circles represent experimental data, while the solid red lines indicate theoretical fitting.

PDA it is 1.06731, representing an enhancement of approximately 117 times in the PDA-based nanofluid. As noted in our previous study, DA can exhibit measurable nonlinearity at higher concentrations; however, in the present case, the DA concentration is relatively low (~261 μM). At such low levels, the contribution of DA to the overall nonlinear response is minimal, yielding an extremely weak signal. In contrast, the PDA-based nanofluid exhibits pronounced nonlinearity, as evidenced by the significantly enhanced ΔT_{P-V}.

This marked enhancement in the nonlinear response can be attributed to the exceptional photothermal conversion efficiency of PDA. When exposed to the 532 nm CW laser, the PDA nanoparticles efficiently absorb photons and convert the absorbed energy into localized heat *via* a nonradiative decay pathway. Additionally, the use of CW excitation ensures a continuous energy supply, preventing sufficient time for thermal dissipation. This sustained heating generates a temperature gradient within the nanofluid as the laser beam propagates through it. The resulting thermal gradient induces a thermal lens effect, causing a spatial variation in the refractive index of the medium. This refractive index modulation leads to phase distortion of the transmitted laser beam, which manifests as the peak–valley profile observed in the CA Z-scan curve.[51–53] Collectively, these findings confirm that PDA-based nanofluid exhibits significant thermally induced optical nonlinearity under CW excitation, a behaviour fundamentally rooted in its high photothermal conversion capability. These results substantiate the potential of PDA-based nanofluids as highly effective materials for photothermal applications.

We also performed the CA Z-scan measurements on the synthesized PDA-based nanofluids under varying incident laser powers to examine their nonlinear photophysical behaviour as a function of laser power. The experimental outcomes, presented in Fig. 4, clearly demonstrate a laser-power-dependent nonlinear response. Specifically, ΔT_{P-V} exhibited an upward trend with increasing laser power. For instance, a 4-fold increase in laser power led to approximately a 2.2-fold enhancement in ΔT_{P-V}, implying a significant amplification of the induced thermal lensing effect at higher laser powers. Furthermore, analysis of all the CA Z-scan profiles consistently showed that the normalized peak transmittance (ΔT_P) exceeded the corresponding valley transmittance (ΔT_V), indicative of the

Table 1 Nonlinear parameters of PDA-based nanofluid under CW laser irradiation at different laser powers

Power (mW)	$-\vartheta(q)$	$-\mathrm{d}n/\mathrm{d}T$ ($\times 10^{-4}$ K^{-1})	$-n_2$ ($\times 10^{-12}$ m^2 W^{-1})
20	1.353	5.411	3.599
40	1.534	3.067	2.040
60	1.708	2.277	1.514
80	1.894	1.894	1.259

presence and contribution of saturable absorption (SA) to the nonlinear response.[29,30,54] Interestingly, upon a 4-fold increase in laser power, ΔT_P and ΔT_V increased by ~1.8 and ~3 times, respectively. This disproportionate growth suggests a diminishing contribution of SA as the laser power rises. Moreover, Fig. 4 provides insight into the normalized peak-to-valley separation distances (Δz_{P-V}). These distances remained around $1.7z_0$ at lower powers [20 mW (Fig. 4(A)) and 40 mW (Fig. 4(B))], characteristic of intrinsic third-order nonlinear processes.[29,30] However, higher powers of 60 mW [Fig. 4(C)] and 80 mW [Fig. 4(D)] displayed increased separations of approximately $2.13z_0$ and $2.5z_0$, respectively. This deviation from the standard third-order nonlinear reference ($\Delta z_{P-V} = 1.7z_0$) at elevated powers clearly indicates an additional nonlinear contribution, predominantly from thermal effects.[53,55]

In the case of CW laser excitation, it is speculated that the nonlinearity arises from changes in a material's optical properties due to heat generated by laser absorption. A temperature gradient is created in the sample due to heat generation, which depends on the material's thermal conductivity and the intensity distribution of the Gaussian laser beam. This temperature gradient might lead to a density variation in the sample under study. The process described above can generate a refractive index (n_2) gradient across the sample, leading to thermal lensing. In turn, Falconieri proposed a model that comprehensively accounts for the thermal effects of the Z-scan technique, while considering higher-order absorption and the aberrated nature of the lens. For the CW regime, the steady-state thermo-optical normalized transmittance ($T(z)$) can be given as[31,52]

$$T(z) = 1 + \frac{\vartheta(q)}{q(1+x^2)^{q-1}} \tan^{-1}\left(\frac{2qx}{2q+1+x^2}\right) \quad (1)$$

where, $x = z/z_0$. The thermal lens strength/on-axis phase shift and the order of absorption are denoted as $\vartheta(q)$ and q, respectively. According to the order of absorption, the corresponding absorption processes for $q = 1$, 2, and 3 are one-photon, two-photon, and three-photon absorption, respectively. The experimental data are theoretically fitted using eqn (1) to get the values of $\vartheta(q)$ and q. The following relations are then utilized to calculate the thermally induced nonlinear refractive index (n_2) and thermo-optical coefficient ($\mathrm{d}n/\mathrm{d}T$) using the fitting parameters:[31,50,53,56]

$$n_2 = \frac{\vartheta(q)}{kI_0L_{\mathrm{eff}}} \quad (2)$$

$$\frac{\mathrm{d}n}{\mathrm{d}T} = \frac{\vartheta(q)\lambda\kappa}{PL\alpha_0} \quad (3)$$

where $k = 2\pi/\lambda$ is the wave vector, $I_0 = 2P/\pi {w_0}^2$ is the on-axis beam irradiance at focus, $L_{\mathrm{eff}} = [1 - \exp(-\alpha_0 L)]/\alpha_0$, κ is the thermal conductivity of the solvent (=0.5918 Wm^{-1} K^{-1}), P is the laser power, w_0 is the beam waist at the focus, and α_0 is the linear absorption coefficient.

Table 1 presents the estimated thermo-optical nonlinear parameters, calculated using eqn (1)–(3). The analysis reveals that $\vartheta(q)$ systematically increases with rising laser power, signifying a strengthening of the nonlinear thermo-optical response at higher intensities, consistent with the observed trend in ΔT_{P-V}. Additionally, the fitting parameter q remained unity across all laser power levels, indicating that the observed nonlinearity arises from a single-photon process.[52] Inspection of Fig. 1 further confirms that the PDA-based nanofluid exhibits significant linear absorption at 532 nm. Consequently, when irradiated with an intense 532 nm laser beam, the SA effect observed in the samples is predominantly attributed to a one-photon absorption mechanism. Here, the measured n_2 magnitudes are of the same order as those reported for processes dominated by saturated atomic absorptive nonlinearity.[57] From Table 1, it is evident that both $\mathrm{d}n/\mathrm{d}T$ and n_2 values decrease with increasing laser power. According to eqn (2) and (3), the magnitudes of n_2 and $\mathrm{d}n/\mathrm{d}T$ are directly proportional to the thermal lens strength $\vartheta(q)$ and inversely proportional to the on-axis intensity (I_0) or the incident laser power (P). Although the thermal lens strength increases with laser power, its rate of increase is considerably lower than that of P and I_0. As a result, the inverse dependence on laser power dominates, leading to a reduction in the calculated values of both n_2 and $\mathrm{d}n/\mathrm{d}T$ at higher laser powers.

Under fs laser excitation. This study examines the nonlinear photophysical behaviour of DA and PDA-based nanofluids using both CA and OA Z-scan techniques under fs laser excitation at two distinct wavelengths (λ_{ex} = 500 nm and 660 nm). The excitation wavelengths of 500 nm and 660 nm were chosen for comparative and application-oriented reasons. The 500 nm wavelength enables direct comparison with CW measurements (532 nm) within the same spectral region, allowing distinction between thermal and ultrafast electronic nonlinearities. In contrast, 660 nm, a wavelength commonly used in photodynamic therapy,[58,59] was employed to investigate the nonlinear response under femtosecond excitation, thereby demonstrating the potential for single-wavelength activation in combined photodynamic and two-photon photothermal therapy. During the measurements, the laser output power was maintained at 100 μW for both 500 nm and 660 nm excitations. The laser operated with a pulse width of 100 fs and a repetition rate of 1 kHz throughout the experiments. The Z-scan results for PDA-based nanofluids, along with those for DA solutions of equal concentration, are depicted in Fig. 5, where the normalized Z-scan traces of both samples are overlaid to enable a direct comparison. Fig. 5 reveals that, across all excitation wavelengths (λ_{ex}), the CA Z-scan profiles exhibit a characteristic valley-peak configuration. This signature is indicative of

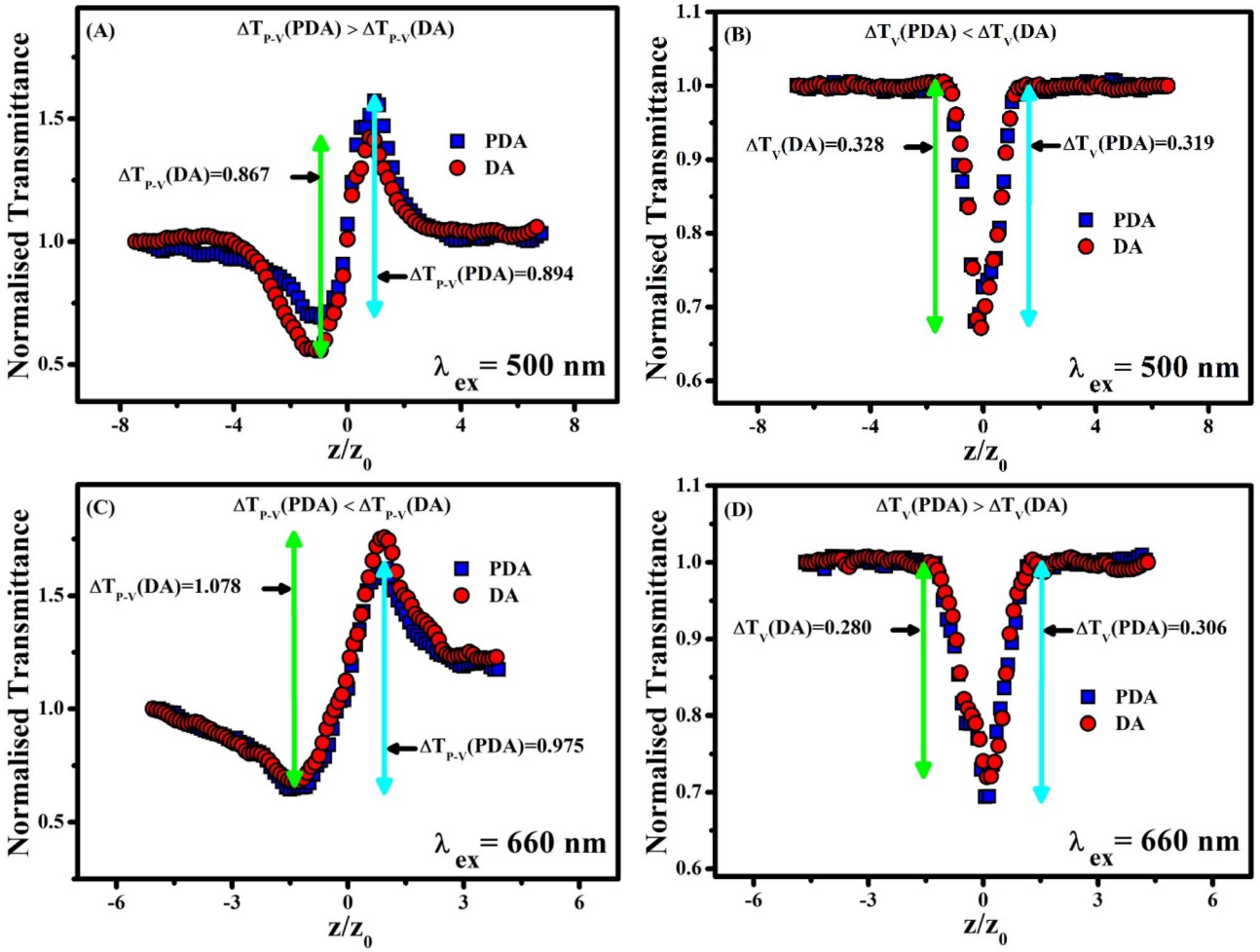

Fig. 5 CA and OA Z-scan traces for pure DA solution and PDA-based nanofluid under femtosecond laser excitation. The laser power was fixed at 100 μW for both 500 nm and 660 nm excitations. Panels (A) and (B) present CA and OA Z-scan signals at 500 nm, while panels (C) and (D) present the corresponding signals at 660 nm.

a positive n_2, arising from self-focusing effects within the DA and PDA-based nanofluid samples.[29,30,32,36] Such behaviour reflects the material's tendency to locally increase its refractive index under intense optical fields, thereby converging the incident beam. The OA Z-scan traces at both 500 nm and 660 nm excitations exhibit a distinct valley, corresponding to a positive nonlinear absorption coefficient (β). This positive β value signifies the dominance of reverse saturable absorption (RSA).[29,30,40]

From Fig. 5, it is clear that for the CA Z-scan signals, ΔT_{P-V} is 0.894 for PDA and 0.867 for DA at a laser excitation wavelength of 500 nm. At 660 nm excitation, ΔT_{P-V} is 0.975 for PDA and 1.078 for DA. For the OA Z-scan signals, ΔT_V is 0.319 for PDA and 0.328 for DA at 500 nm, while at 660 nm it is 0.306 for PDA and 0.280 for DA. These observations show that, at identical concentrations, the ΔT_{P-V} values from the CA Z-scan, as well as the ΔT_V values from the OA Z-scan, exhibit no significant differences between DA and PDA-based nanofluids across the tested wavelengths. This indicates that PDA-based nanofluids do not exhibit a measurable enhancement in optical nonlinearity under fs laser excitation, as observed in both CA and OA Z-scan profiles. A probable explanation for this behaviour is that PDA polymerization does not introduce additional ultrafast nonlinear pathways beyond those inherently present in DA monomers, resulting in no change of the femtosecond-scale Z-scan response. In contrast, under CW laser excitation, PDA-based nanofluid exhibits markedly different behaviour. PDA nanoparticles in the nanofluid strongly absorb CW radiation, efficiently converting it into localized heat and thereby inducing prominent thermal effects, which significantly amplify the Z-scan signals. Although the PDA-based nanofluid does not exhibit a measurable enhancement in nonlinear optical response compared to DA on the femtosecond scale, its broader significance lies in the unique and versatile properties of PDA. PDA is renowned for its exceptional and universal surface adhesion, extensive chemical reactivity, intrinsic biocompatibility and biodegradability, remarkable drug-loading capacity, and excellent photothermal conversion efficiency.[1,2,5,6] Given these extraordinary characteristics, it remains essential to investigate the nonlinear optical properties of PDA

Table 2 Nonlinear parameters of PDA-based nanofluid under fs laser irradiation at different excitation wavelengths

Wavelength (λ) (nm)	n_2 ($\times 10^{-19}$ m^2 W^{-1})	β ($\times 10^{-13}$ mW^{-1})	$\chi_R^{(3)}$ ($\times 10^{-21}$ m^2 V^{-2})	$\chi_I^{(3)}$ ($\times 10^{-22}$ m^2 V^{-2})	$\lvert\chi^{(3)}\rvert$ ($\times 10^{-21}$ m^2 V^{-2})
500	2.725	145.935	2.560	54.575	6.028
660	7.224	55.783	6.789	27.537	7.326

on the femtosecond scale, as insights from such studies could help in designing next-generation optical materials and devices for advanced technological and biomedical applications.

Since the comparative measurements revealed no significant difference in the nonlinear response between DA and PDA-based nanofluids, DA was excluded from further nonlinear parameter evaluation. The study, therefore, focuses exclusively on PDA-based nanofluids to comprehensively assess and quantify their nonlinear optical parameters. Given that our samples were investigated using an ultrashort laser pulse, any thermal effects on the nonlinear response are expected to be negligible. Under these circumstances, the Sheik-Bahae formalism is well-suited for analyzing the data. A key assumption of this model is that the light–matter interaction is local, so the nonlinear susceptibility is determined solely by the instantaneous intensity of the incident beam. To improve the theoretical description of the Z-scan technique, Sheik-Bahae and co-workers employed a Gaussian decomposition approach. When the thin-sample condition is satisfied, and the measurement is carried out in the low-irradiance limit with a small aperture and minimal phase distortion, the normalized transmittance $T(z)$ for a closed-aperture Z-scan can be written, to first order, as:[29,30,43,50]

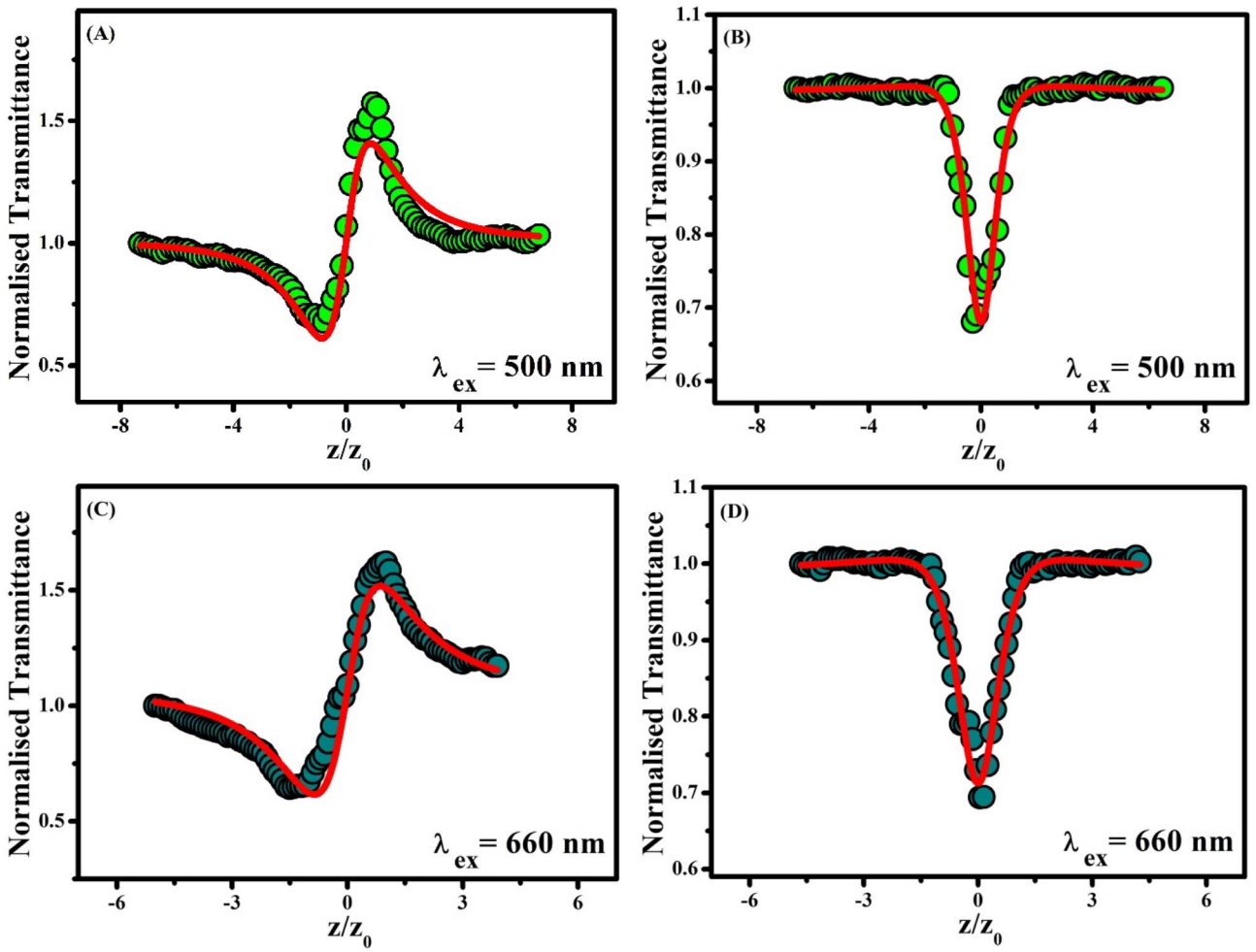

Fig. 6 CA and OA Z-scan profiles of PDA-based nanofluid recorded under fs laser excitation, with laser powers set to 100 μW for 500 nm and 660 nm. Panels (A) and (B) present CA and OA Z-scan signals at 500 nm, while panels (C) and (D) present the corresponding signals at 660 nm. The closed circles represent experimental data, and the solid red lines indicate the theoretical fit.

$$T(z) = 1 + \frac{4x}{(x^2+1)(x^2+9)}\Delta\phi_0 \quad (4)$$

$x = z/z_0$ and $\Delta\phi_0$ is the phase shift due to nonlinear refraction.

$$\Delta\phi_0 = kn_2 I_0 L_{\text{eff}} \quad (5)$$

The OA Z-scan data were analyzed using the appropriate expression for the normalized transmittance, which is given as follows:[29,60,61]

$$T(z) = 1 - \frac{\alpha_0 L_{\text{eff}}}{1 + \frac{I_0}{(1+x^2)I_s}} - \frac{\beta I_0 L_{\text{eff}}}{1+x^2} \quad (6)$$

I_S is the saturation intensity, and β is the nonlinear absorption coefficient.

The following expressions are used to extract the real ($\chi_R^{(3)}$) and imaginary ($\chi_I^{(3)}$) parts of the third-order nonlinear optical susceptibility, as well as its overall magnitude $|\chi^{(3)}|$.[29,50,55] The calculated values of these parameters are summarized in Table 2.

$$\chi_R^{(3)} = 2n_0^2\epsilon_0 c n_2 \quad (7)$$

$$\chi_I^{(3)} = \frac{n_0^2\epsilon_0 c\lambda\beta}{2\pi} \quad (8)$$

$$|\chi^{(3)}| = \sqrt{|\chi_R^{(3)}|^2 + |\chi_I^{(3)}|^2} \quad (9)$$

where n_0 is the linear refractive index of the solvent, $\epsilon_0 = 8.854 \times 10^{-12}$ Fm^{-1} is the permittivity of free space, and $c = 3 \times 10^8$ ms^{-1} is the speed of light in vacuum.

To determine the nonlinear optical parameters, the CA Z-scan data for the PDA-based nanofluid were first normalized by dividing them by the corresponding OA Z-scan data. This CA/OA ratio isolates the purely refractive nonlinear contribution by eliminating the influence of nonlinear absorption. The resulting normalized data were then fitted using eqn (4) to extract the n_2 values. In parallel, the OA Z-scan data were analyzed using eqn (6) to estimate the β values. Fig. 6 presents the CA and OA Z-scan experimental results along with their corresponding theoretical model fits by eqn (4), and (6), respectively. The n_2 is obtained from eqn (5), and β is obtained directly from eqn (6) as a fitting parameter. Finally, the $|\chi^{(3)}|$, was subsequently calculated using eqn (7)–(9). The compiled nonlinear parameters (n_2, β, and $|\chi^{(3)}|$) are presented in Table 2.

Table 2 reveals that the n_2 and β values remain positive across all investigated wavelengths, indicating a consistent self-focusing and RSA behaviour of the PDA-based nanofluids.[29,30,32,55] This RSA behaviour can be explained by considering the linear absorption profile of PDA-based nanofluids. As evident from Fig. 1, the samples exhibit substantial linear absorption at wavelengths corresponding to half of 500 nm and 660 nm. Additionally, under femtosecond excitation (100 fs), the pulse duration is much shorter than the excited-state lifetimes (ps-ns), which suppresses excited-state and sequential absorption, while the low repetition rate (1 kHz) ensures complete thermal relaxation between pulses, eliminating thermal contributions. Consequently, the applied femtosecond laser excitations facilitate two-photon absorption (TPA), leading to the observed RSA behaviour at these wavelengths. Furthermore, the magnitudes of these parameters indicate that the observed nonlinearity is predominantly driven by an electronic polarization mechanism, consistent with the ultrafast response expected under femtosecond excitation.[57]

Optical power limiting study

The normalized transmittance, $T(z)$, of a material is defined as the ratio of the transmitted intensity to the incident intensity. By plotting $T(z)$ as a function of input fluence, valuable insights into the material's optical power limiting (OPL) behaviour can be gained. A progressive decrease in $T(z)$ with increasing input fluence is typically indicative of an onset of optical power limiting, as the material begins to attenuate the transmitted light at higher excitation laser powers. This relationship provides a straightforward yet powerful method for assessing the suitability of materials for photonic protection and high-intensity laser safety applications.[62–66]

The OPL behaviour of the PDA-based nanofluid was further evaluated using the OA Z-scan data. The relationship between the OA normalized transmittance and input fluence is presented in Fig. 7, providing direct insight into the sample's OPL behaviour at 500 nm and 660 nm excitation wavelengths. To obtain the position-dependent input fluence, $F_{\text{in}}(z)$, the OA data were analyzed using the standard expression: $F_{\text{in}}(z) = 4(\ln 2)^{1/2}E_{\text{in}}/(\pi^{3/2}w_0^2(1+x^2))$, where E_{in} represents the input pulse energy.[67–69] This calculation enabled accurate mapping of the fluence distribution along the propagation axis, facilitating a clear assessment of the OPL performance of the PDA-based nanofluid under fs excitation. From Fig. 7, it is evident that the normalized transmittance of the PDA-based nanofluid decreases progressively with increasing input fluence, confirming that its OPL behaviour is primarily governed by a two-

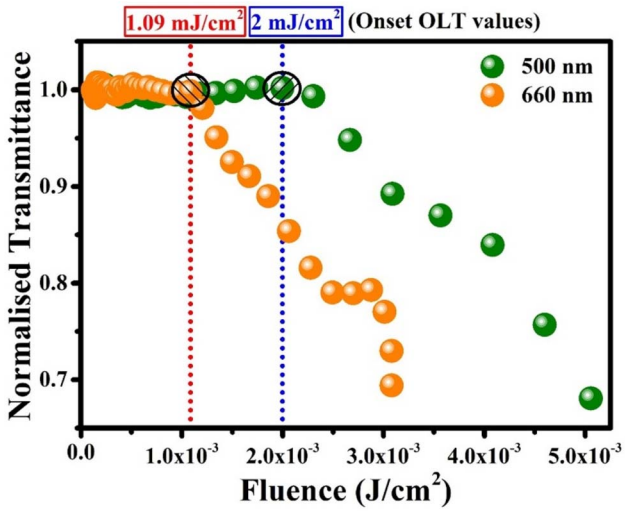

Fig. 7 Optical power limiting (OPL) curves of PDA-based nanofluid under excitation at 500 nm and 660 nm wavelengths.

photon-assisted RSA mechanism. Analysis of the OPL curves further reveals that the transmittance remains nearly linear at lower fluence levels but decreases once the fluence exceeds a threshold. This transition point, where the linear response shifts to a nonlinear regime, is defined as the onset optical limiting threshold (OLT).[63] The measured onset OLT values were found to be 2 mJ cm^{-2} for 500 nm excitation and 1.09 mJ cm^{-2} for 660 nm excitation. These thresholds mark the input fluence levels beyond which the PDA-based nanofluid effectively begins to attenuate high-intensity light, demonstrating its potential as an optical limiting material for laser protection applications.

Conclusions

In summary, this work reports the successful synthesis of PDA-based nanofluid through the oxidative self-polymerization of DA under mildly alkaline conditions. The formation of PDA nanoparticles was initially confirmed by the broad UV-vis absorption spectrum, which also indicated their stable dispersion in the solvent, leading to the formation of a well-dispersed PDA-based nanofluid. HRTEM study further validated the presence of nanoparticles in the nanometer range (~4 nm). CA Z-scan measurements under CW laser excitation revealed a negative n_2 value, signifying the self-defocusing nature of the PDA-based nanofluid. Additionally, a substantial enhancement in the thermo-optical nonlinearity was observed, which is attributable to the high photothermal conversion efficiency of PDA. These thermo-optical nonlinear parameters were systematically extracted through a power-dependent study, highlighting the strong thermal contribution under CW excitation. To investigate ultrafast nonlinear optical responses, a fs laser excitation was employed for both CA and OA Z-scan studies at 500 nm and 660 nm. CA Z-scan measurements under fs excitation revealed a positive n_2 value across two wavelengths, indicating a self-focusing response. Meanwhile, the OA Z-scan measurements yielded a positive β value, indicative of two-photon-assisted RSA. The OPL performance of the PDA-based nanofluid was further evaluated, revealing onset OLT values of 2 mJ cm^{-2} at 500 nm and 1.09 mJ cm^{-2} at 660 nm. These results underscore the material's capability to attenuate high-intensity laser radiation, positioning it as a strong candidate for optical limiting applications.

Overall, the findings of this research suggest that PDA-based nanofluid holds significant promise as a multifunctional material. Although PDA-based nanofluid and DA exhibit similar behavior under femtosecond excitation, indicating comparable two-photon absorption, PDA offers a clear advantage due to its significantly higher photothermal conversion efficiency. Its dual characteristics of high photothermal conversion efficiency and two-photon absorption at 660 nm make it an excellent prospect for two-photon photothermal cancer therapy. As a result, despite similar ultrafast nonlinear responses, PDA is more effective for two-photon photothermal cancer therapy because it converts absorbed energy into heat more efficiently. This enables spatially confined energy deposition through two-photon absorption, allowing precise thermal modulation with enhanced penetration depth and reduced collateral effects. Meanwhile, its OPL behavior demonstrates potential for use in laser safety, optical protection systems, and all-optical switching technologies. Such properties make it suitable for the development of compact optical limiting devices capable of protecting sensitive sensors and human eyes from high-intensity laser exposure. This study provides one of the first comprehensive evaluations of nonlinear photophysical parameters of PDA-based nanofluid under both CW and fs excitations, paving the way for their integration into biomedical platforms, next-generation photonics, and optoelectronic devices.

Experimental section

Synthesis of polydopamine (PDA)-based nanofluid

Polydopamine-based nanofluid (PDA-based nanofluid) was synthesized *via* the oxidative self-polymerization of dopamine (DA) under mildly alkaline conditions. A 261 μM DA solution was prepared in a 6 : 4 (v/v) water–ethanol mixture. To begin the polymerization, 0.5 M NaOH solution was added dropwise to the DA solution under continuous stirring using a TARSONS DIGITAL SPINOT (Pt-1000), India magnetic stirrer set at 500 rpm. The final concentration of NaOH in solution was 1.32 mM. A visible colour change from colourless to straw yellow was observed instantly after the addition of NaOH. The introduction of NaOH initiated the self-polymerization of DA, leading to the formation of PDA nanoparticles (PDA NPs) in the solution. After stirring for 1 hour, a stable, light-brown-colored dispersion of PDA NPs was obtained. These PDA NPs dispersed in the solution are collectively referred to as PDA-based nanofluid. Fig. 8 shows the schematic route for PDA-based nanofluid synthesis. The PDA-based nanofluid was directly used as prepared in a 6 : 4 (v/v) water–ethanol mixture, without any additional separation or redispersion. The successful synthesis was confirmed through UV-visible absorption spectroscopy, while the particle size and morphology were characterized using high-resolution transmission electron microscopy (HRTEM).

Sample characterization

Ultraviolet-visible (UV-vis) absorption spectroscopy. In this study, UV-visible absorption spectra of DA and PDA were obtained using a UV-visible spectrophotometer (Shimadzu UV-2600, Japan). Spectral measurements were carried out using

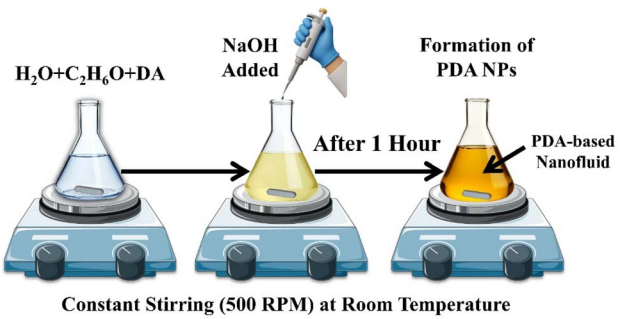

Fig. 8 Schematic route for PDA-based nanofluid synthesis.

a 1 mm quartz cuvette, and the nonlinear parameters were subsequently derived from the corresponding linear absorption coefficients.

High-resolution transmission electron microscopy (HRTEM). In this work, high-resolution imaging was performed using a Talos F200X G2 HRTEM (Thermo Fisher Scientific, USA) operating at 200 kV, providing high-resolution images with superior clarity.

The Z-scan technique. The nonlinear photophysical properties of DA and PDA-based nanofluid were examined using the Z-scan technique under both continuous-wave (CW) and femtosecond (fs) laser excitations. Details of the Z-scan experimental setup developed in our laboratory are provided elsewhere.[33,36,37]

Author contributions

Priyadarshi Sahoo: conceptualization, investigation, data curation, formal analysis, validation, visualization, writing – original draft, writing – review & editing. Manika Dandapat: conceptualization, investigation, data curation, formal analysis, validation, visualization, funding acquisition, writing – review & editing. Amit Kumar Pradhan: investigation, data curation, validation, formal analysis. Prasanta Kumar Datta: validation, supervision, resources, project administration, funding acquisition. Umakanta Tripathy: conceptualization, supervision, validation, project administration, resources, funding acquisition, writing – review & editing.

Conflicts of interest

The authors declare no competing financial interest.

Data availability

The data underlying this study are available in the published article.

Acknowledgements

The authors thank the UPM (SGDRI) project of IIT Kharagpur for providing the femtosecond laser facility. We are grateful to the Science and Engineering Research Board (SERB), DST, New Delhi, India (EMR/2017/003759), for their financial support. The authors also acknowledge the financial assistance from the DST WOS-A (DST/WOS-A/CS-18/2021). In accordance with RSC guidelines on the use of AI tools, we acknowledge that ChatGPT was used during manuscript preparation for grammar checking, paraphrasing, and language editing.

References

1 H. Li, D. Yin, W. Li, Q. Tang, L. Zou and Q. Peng, *Colloids Surf., B*, 2021, **199**, 111502.
2 H. Li, Y. Jia, H. Peng and J. Li, *Adv. Colloid Interface Sci.*, 2018, **252**, 1–20.
3 S. Song, W. Zhu, C. Long, Y. Zhang, S. Chen and L. Dong, *Eur. J. Inorg. Chem.*, 2016, **2016**, 148–153.
4 Y. Liu, K. Ai and L. Lu, *Chem. Rev.*, 2014, **114**, 5057–5115.
5 M. E. Lynge, P. Schattling and B. Städler, *Nanomedicine*, 2015, **10**, 2725–2742.
6 M. Liu, G. Zeng, K. Wang, Q. Wan, L. Tao, X. Zhang and Y. Wei, *Nanoscale*, 2016, **8**, 16819–16840.
7 A. R. K. Sasikala, A. GhavamiNejad, A. R. Unnithan, R. G. Thomas, M. Moon, Y. Y. Jeong, C. H. Park and C. S. Kim, *Nanoscale*, 2015, **7**, 18119–18128.
8 H. Zhuang, H. Su, X. Bi, Y. Bai, L. Chen, D. Ge, W. Shi and Y. Sun, *ACS Biomater. Sci. Eng.*, 2017, **3**, 1799–1808.
9 T. Bedhiafi, S. Idoudi, A. A. Alhams, Q. Fernandes, H. Iqbal, R. Basineni, S. Uddin, S. Dermime, M. Merhi and N. Billa, *J. Controlled Release*, 2023, **353**, 842–849.
10 P. Zheng, B. Ding and G. Li, *Macromol. Biosci.*, 2020, **20**, 2000228.
11 D. R. Dreyer, D. J. Miller, B. D. Freeman, D. R. Paul and C. W. Bielawski, *Langmuir*, 2012, **28**, 6428–6435.
12 R. Zheng, S. Wang, Y. Tian, X. Jiang, D. Fu, S. Shen and W. Yang, *ACS Appl. Mater. Interfaces*, 2015, **7**, 15876–15884.
13 P. Zhang, X. Li, Q. Xu, Y. Wang and J. Ji, *Colloids Surf., B*, 2021, **208**, 112125.
14 Z. Zhao, H. Zhang, H. Chen, Y. Xu, L. Ma and Z. Wang, *J. Mater. Chem. B*, 2022, **10**, 4012–4019.
15 C. Chen, W. Tang, D. Jiang, G. Yang, X. Wang, L. Zhou, W. Zhang and P. Wang, *Nanoscale*, 2019, **11**, 11012–11024.
16 D. Khurana, Vikas, A. K. Shaw and S. Soni, *IEEE Trans. NanoBiosci.*, 2022, **21**, 482–489.
17 C. Wei, P. Wang, Z. Huang, D. He, W. Zhu, H. Liu, Z. Chen, W. Wang, Y. Li, J. Shen and L. Qin, *Mol. Pharm.*, 2021, **18**, 1327–1343.
18 J. H. Ryu, P. B. Messersmith and H. Lee, *ACS Appl. Mater. Interfaces*, 2018, **10**, 7523–7540.
19 L. Wang and L. Zhang, *Polym. Bull.*, 2025, **82**, 375–395.
20 L. Lv, H. Cheng, Z. Wang, Z. Miao, F. Zhang, J. Chen, G. Wang, L. Tao, J. Zhou, H. Zhang and Y. Ding, *Nanoscale*, 2022, **14**, 13740–13754.
21 L. Wang and J. Liu, *Acc. Chem. Res.*, 2024, **57**, 945–956.
22 M. L. Alfieri, L. Panzella and A. Napolitano, *Eur. J. Org Chem.*, 2024, **27**, e202301002.
23 Y. Li, Y. Cheng, Y. Wu, Z. Wang, X. Ma, J. Zhao, Z. Yang and Y. Ji, *Ind. Eng. Chem. Res.*, 2024, **63**, 3140–3151.
24 Y. Zhu, J. Ling, X. Xu, X.-k. Ouyang and N. Wang, *Int. J. Biol. Macromol.*, 2023, **240**, 124488.
25 W. Lei, C. Sun, T. Jiang, Y. Gao, Y. Yang, Q. Zhao and S. Wang, *Mater. Sci. Eng., C*, 2019, **105**, 110103.
26 R. Zhang, S. Su, K. Hu, L. Shao, X. Deng, W. Sheng and Y. Wu, *Nanoscale*, 2015, **7**, 19722–19731.
27 R. S. Ambekar and B. Kandasubramanian, *Biomater. Sci.*, 2019, **7**, 1776–1793.
28 S. Geng, Q. Feng, C. Wang, Y. Li, J. Qin, M. Hou, J. Zhou, X. Pan, F. Xu, B. Fang, K. Wang and Z. Yu, *J. Nanobiotechnol.*, 2023, **21**, 338.
29 M. Sheik-Bahae, A. A. Said, T. H. Wei, D. J. Hagan and E. W. V. Stryland, *IEEE J. Quantum Electron.*, 1990, **26**, 760–769.
30 M. Sheik-Bahae, A. A. Said and E. W. Van Stryland, *Opt. Lett.*, 1989, **14**, 955–957.

31 P. Sahoo, N. K. Pathak, D. Scott Bohle, E. L. Dodd and U. Tripathy, *Spectrochim. Acta, Part A*, 2024, **310**, 123902.
32 D. Paul, P. Sahoo, A. K. Pradhan, P. K. Datta, A. Sengupta, U. Tripathy and S. Chatterjee, *J. Chem. Phys.*, 2025, **162**, 234308.
33 N. K. Pathak, P. Sahoo and U. Tripathy, *Talanta*, 2024, **272**, 125808.
34 D. Paul, P. Sahoo, A. Sengupta, U. Tripathy and S. Chatterjee, *J. Phys. Chem. B*, 2025, **129**, 692–711.
35 N. K. Pathak, P. Sahoo and U. Tripathy, in *Biochemical and Biophysical Methods in Molecular and Cellular Biology*, ed. U. Tripathy, Springer Nature Singapore, Singapore, 2025, pp. 117–139, DOI: 10.1007/978-981-96-2088-3_5.
36 N. K. Pathak, Nandeshwar, P. Sahoo, A. K. Pradhan, T. Singha, P. K. Datta and U. Tripathy, *Sci. Rep.*, 2025, **15**, 34240.
37 P. Sahoo, N. K. Pathak, S. K. Verma and U. Tripathy, *J. Appl. Phys.*, 2025, **138**, 074701.
38 S. Zhang, N. Dong, N. McEvoy, M. O'Brien, S. Winters, N. C. Berner, C. Yim, Y. Li, X. Zhang, Z. Chen, L. Zhang, G. S. Duesberg and J. Wang, *ACS Nano*, 2015, **9**, 7142–7150.
39 J. Yu, E. G. Durmusoglu, Y. Ren, W. Fang, Y. Zhou, L. Chu, B. Liu and H. V. Demir, *ACS Nano*, 2025, **19**, 9273–9281.
40 K. Wang, J. Wang, J. Fan, M. Lotya, A. O'Neill, D. Fox, Y. Feng, X. Zhang, B. Jiang, Q. Zhao, H. Zhang, J. N. Coleman, L. Zhang and W. J. Blau, *ACS Nano*, 2013, **7**, 9260–9267.
41 L. Gao, H. Chen, A. V. Kuklin, S. Wageh, A. A. Al-Ghamdi, H. Ågren and H. Zhang, *ACS Nano*, 2022, **16**, 3059–3069.
42 E. Van Stryland and M. Sheik-Bahae, *Z-Scan Technique for Nonlinear Materials Characterization*, SPIE, 1997.
43 M. Yin, H. P. Li, S. H. Tang and W. Ji, *Appl. Phys. B*, 2000, **70**, 587–591.
44 J. Liebscher, R. Mrówczyński, H. A. Scheidt, C. Filip, N. D. Hădade, R. Turcu, A. Bende and S. Beck, *Langmuir*, 2013, **29**, 10539–10548.
45 M. d'Ischia, A. Napolitano, V. Ball, C.-T. Chen and M. J. Buehler, *Acc. Chem. Res.*, 2014, **47**, 3541–3550.
46 K.-Y. Ju, M. C. Fischer and W. S. Warren, *ACS Nano*, 2018, **12**, 12050–12061.
47 C.-T. Chen, V. Ball, J. J. de Almeida Gracio, M. K. Singh, V. Toniazzo, D. Ruch and M. J. Buehler, *ACS Nano*, 2013, **7**, 1524–1532.
48 Y. Zou, X. Chen, P. Yang, G. Liang, Y. Yang, Z. Gu and Y. Li, *Sci. Adv.*, 2020, **6**, eabb4696.
49 Sakshi, B. C. Swain, A. K. Das, N. K. Pathak and U. Tripathy, *Spectrochim. Acta, Part A*, 2022, **271**, 120890.
50 U. Tripathy and P. B. Bisht, *J. Opt. Soc. Am. B*, 2007, **24**, 2147–2156.
51 A. Gnoli, L. Razzari and M. Righini, *Opt. Express*, 2005, **13**, 7976–7981.
52 F. Mauro, *J. Opt. A: Pure Appl. Opt.*, 1999, **1**, 662.
53 F. L. S. A. Cuppo, A. M. Figueiredo Neto, S. L. Gómez and P. Palffy-Muhoray, *J. Opt. Soc. Am. B*, 2002, **19**, 1342–1348.
54 Sakshi, B. C. Swain, A. K. Das and U. Tripathy, *Spectrochim. Acta, Part A*, 2019, **223**, 117319.
55 N. K. Pathak, L. Sharma, Sakshi, B. Panda and U. Tripathy, *Opt. Mater.*, 2022, **126**, 112230.
56 Sakshi, N. K. Pathak, B. C. Swain and U. Tripathy, *Opt Laser. Technol.*, 2020, **121**, 105822.
57 R. W. Boyd, A. L. Gaeta and E. Giese, in *Springer Handbook of Atomic, Molecular, and Optical Physics*, ed. G. W. F. Drake, Springer International Publishing, Cham, 2023, pp. 1097–1110, DOI: 10.1007/978-3-030-73893-8_76.
58 F. Wu, Y. Liu, Y. Wu, D. Song, J. Qian and B. Zhu, *J. Mater. Chem. B*, 2020, **8**, 2128–2138.
59 S. Yan, L. Dong, Z. Hu, Y. Zhang, W. Xu, J. Xing and J. Zhang, *Molecules*, 2023, **28**, 5874.
60 C. Chen, J. Wang and Y. Gao, *Appl. Sci.*, 2021, **11**, 1640.
61 V. Sreeramulu, K. K. Haldar, A. Patra and D. N. Rao, *J. Phys. Chem. C*, 2014, **118**, 30333–30341.
62 R. K. Rohal, J. N. Acharyya, M. Shanu, G. V. Prakash and M. Sankar, *Inorg. Chem.*, 2022, **61**, 1297–1307.
63 S. R. Maidur, P. S. Patil, N. K. Katturi, V. R. Soma, Q. Ai Wong and C. K. Quah, *J. Phys. Chem. B*, 2021, **125**, 3883–3898.
64 S. Biswas, A. K. Kole, C. S. Tiwary and P. Kumbhakar, *RSC Adv.*, 2016, **6**, 10319–10325.
65 C. Zheng, W. Chen, Y. Huang, X. Xiao and X. Ye, *RSC Adv.*, 2014, **4**, 39697–39703.
66 S. Sirohi, D. Ray Chawdhury, S. Narayanan and P. B. Bisht, *ACS Appl. Nano Mater.*, 2025, **8**, 254–264.
67 G. Lepcha, T. Singha, S. Majumdar, A. K. Pradhan, K. S. Das, P. K. Datta and B. Dey, *Dalton Trans.*, 2022, **51**, 13435–13443.
68 R. Philip, P. Chantharasupawong, H. Qian, R. Jin and J. Thomas, *Nano Lett.*, 2012, **12**, 4661–4667.
69 S. Biswas, A. K. Kole and P. Kumbhakar, *Chem. Phys. Lett.*, 2015, **629**, 70–75.